The Astrophysical Journal, 831:142 (8pp), 2016 November 10 doi:10.3847/0004-637X/831/2/142

FIRST *NuSTAR* OBSERVATIONS OF THE BL LAC-TYPE BLAZAR PKS 2155-304: CONSTRAINTS ON THE JET CONTENT AND DISTRIBUTION OF RADIATING PARTICLES

G. M. Madejski[1], K. Nalewajko[1,2], K. K. Madsen[3], J. Chiang[1], M. Baloković[3], D. Paneque[4], A. K. Furniss[1,5], M. Hayashida[6], C. M. Urry[7], M. Sikora[2], M. Ajello[8], R. D. Blandford[1], F. A. Harrison[3], D. Sanchez[9], B. Giebels[10], D. Stern[11], D. M. Alexander[12], D. Barret[13,14], S. E. Boggs[15], F. E. Christensen[16], W. W. Craig[15,17], K. Forster[3], P. Giommi[18], B. Grefenstette[3], C. Hailey[19], A. Hornstrup[16], T. Kitaguchi[20], J. E. Koglin[1], P. H. Mao[3], H. Miyasaka[3], K. Mori[19], M. Perri[18,21], M. J. Pivovaroff[17], S. Puccetti[18,21], V. Rana[3], N. J. Westergaard[16], W. W. Zhang[22], and A. Zoglauer[15]

[1] Kavli Institute for Particle Astrophysics and Cosmology, Department of Physics and SLAC National Accelerator Laboratory, Stanford University, Stanford, CA 94305, USA
[2] Nicolaus Copernicus Astronomical Center, Polish Academy of Sciences, Bartycka 18, 00-716 Warsaw, Poland
[3] Cahill Center for Astronomy and Astrophysics, Caltech, Pasadena, CA 91125, USA
[4] Max-Planck-Institut fur Physik, D-80805 Munchen, Germany
[5] California State University—East Bay, 25800 Carlos Bee Boulevard, Hayward, CA 94542, USA
[6] Institute for Cosmic Ray Research, University of Tokyo, 5-1-5 Kashiwanoha, Kashiwa, Chiba, 277-8582, Japan
[7] Yale Center for Astronomy and Astrophysics, Physics Department, Yale University, P.O. Box 208120, New Haven, CT 06520-8120, USA
[8] Department of Physics and Astronomy, Clemson University, Kinard Lab of Physics, Clemson, SC 29634-0978, USA
[9] Laboratoire d'Annecy-le-Vieux de Physique des Particules, Universite de Savoie, CNRS/IN2P3, F-74941 Annecy-le-Vieux, France
[10] Laboratoire Leprince-Ringuet, Ecole Polytechnique, CNRS/IN2P3, F-91128 Palaiseau, France
[11] Jet Propulsion Laboratory, California Institute of Technology, Pasadena, CA 91109, USA
[12] Department of Physics, Durham University, Durham DH1 3LE, UK
[13] Universite de Toulouse, UPS—OMP, IRAP, Toulouse, France
[14] CNRS, Institut de Recherche en Astrophysique et Plantologie, 9 Av. Colonel Roche, BP 44346, F-31028 Toulouse Cedex 4, France
[15] Space Science Laboratory, University of California, Berkeley, CA 94720, USA
[16] DTU Space, National Space Institute, Technical University of Denmark, Elektrovej 327, DK-2800 Lyngby, Denmark
[17] Lawrence Livermore National Laboratory, Livermore, CA 94550, USA
[18] ASI Science Data Center, Via del Politecnico snc I-00133, Roma, Italy
[19] Columbia Astrophysics Laboratory, Columbia University, New York, NY 10027, USA
[20] RIKEN, Nishina Center, 2-1 Hirosawa, Wako, Saitama, 351-0198, Japan
[21] INAF—Osservatorio Astronomico di Roma, via di Frascati 33, I-00040 Monteporzio, Italy
[22] NASA Goddard Space Flight Center, Greenbelt, MD 20771, USA

Received 2016 August 2; revised 2016 August 25; accepted 2016 August 29; published 2016 November 3

ABSTRACT

We report the first hard X-ray observations with *NuSTAR* of the BL Lac-type blazar PKS 2155-304, augmented with soft X-ray data from *XMM-Newton* and γ-ray data from the *Fermi* Large Area Telescope, obtained in 2013 April when the source was in a very low flux state. A joint *NuSTAR* and *XMM* spectrum, covering the energy range 0.5–60 keV, is best described by a model consisting of a log-parabola component with curvature $\beta = 0.3^{+0.2}_{-0.1}$ and a (local) photon index 3.04 ± 0.15 at photon energy of 2 keV, and a hard power-law tail with photon index 2.2 ± 0.4. The hard X-ray tail can be smoothly joined to the quasi-simultaneous γ-ray spectrum by a synchrotron self-Compton component produced by an electron distribution with index $p = 2.2$. Assuming that the power-law electron distribution extends down to $\gamma_{\rm min} = 1$ and that there is one proton per electron, an unrealistically high total jet power of $L_{\rm p} \sim 10^{47}\,{\rm erg\,s^{-1}}$ is inferred. This can be reduced by two orders of magnitude either by considering a significant presence of electron–positron pairs with lepton-to-proton ratio $n_{\rm e+e-}/n_{\rm p} \sim 30$, or by introducing an additional, low-energy break in the electron energy distribution at the electron Lorentz factor $\gamma_{\rm br1} \sim 100$. In either case, the jet composition is expected to be strongly matter-dominated.

Key words: BL Lacertae objects: individual (PKS 2155-304) – galaxies: active – galaxies: jets – gamma rays: galaxies – radiation mechanisms: non-thermal

1. INTRODUCTION

PKS 2155-304 is one of the most extensively studied BL Lac objects. It is a strong emitter of electromagnetic radiation in all observable bands, from radio to very high energy (VHE) γ-rays. Its $E \times F(E)$ broadband spectrum reveals two prominent peaks located, respectively, in the far-UV/soft X-ray band, and in the multi-GeV part of the high-energy γ-ray band. As such, PKS 2155-304 belongs to the class of jet-dominated active galaxies with the jet pointing close to our line of sight—known as blazars—and, specifically, to a sub-class known as high-energy peaked BL Lac objects, or HBLs (see, e.g., Padovani & Giommi 1995).

The two-peak spectral energy distribution (SED) of HBL blazars is generally (and most successfully) interpreted in the context of leptonic synchrotron self-Compton (SSC) models (e.g., Ghisellini et al. 1998), where the low-energy component is presumably due to synchrotron emission, while the high-energy component is due to inverse-Compton scattering by the same electrons that produce the synchrotron peak. The optical spectra of the HBL blazars are generally devoid of emission lines even in the low jet flux states, implying a rather weak isotropic radiation field associated with the accretion. In such objects, it is generally believed that the dominant population of "seed" photons (as seen in the comoving frame of the

relativistic jet) are the synchrotron photons produced within the jet.

From an observational standpoint, in HBL-type blazars perhaps the least is known about the lowest energy part of the inverse-Compton peak. This is primarily due to the limited sensitivity of instruments in the relevant energy range, from ∼20 keV to ∼100 MeV. In particular, the onset of the high-energy peak contains important information about the lowest energy electrons in the jet, which, in the context of any emission model, are most plentiful, and thus are a sensitive probe of the total content of particles in the jet. Notably, this low-energy end of the electron population cannot be reliably studied in the synchrotron component, since at low energies, the synchrotron emission is likely self-absorbed. Fortunately, the successful launch of the *NuSTAR* mission, sensitive in the 3–79 keV energy range, opened a new window for sensitive searches for the low-energy "tail" of the electron distribution in the inverse-Compton component.

In this paper, we report *NuSTAR* observations of PKS 2155-304, one of the brightest and also most luminous HBL blazars. This object, at $z = 0.116$, has been known as a bright X-ray emitter since its discovery by *HEAO*-1 A3 (Schwartz et al. 1979). Subsequent X-ray observations consistently show soft X-ray spectra, with photon index $\Gamma > 2.5$ in the 2–10 keV band (e.g., Sembay et al. 1993; Brinkmann et al. 1994; Edelson et al. 1995; Urry et al. 1997; Zhang et al. 1999; Kataoka et al. 2000; Tanihata et al. 2001; Bhagwan et al. 2014). Rapid variability on hourly timescales in the X-ray and optical bands is common; see Zhang et al. (1999), Edelson et al. (2001), Tanihata et al. (2001), and Kataoka et al. (2000). PKS 2155-304 is a known bright VHE γ-ray source (Chadwick et al. 1999; Aharonian et al. 2005) and is highly variable on timescales down to ∼ minutes in the VHE γ-rays (Aharonian et al. 2007). For the most recent multi-band observations involving *Fermi*-LAT and VHE observatories, see Aharonian et al. (2009) or Chevalier et al. (2015).

NuSTAR observed PKS 2155-304 multiple times in 2013, as a part of multi-frequency monitoring with ground-based observatories, spanning radio through VHE bands. Here, we focus on the X-ray spectroscopy afforded by the first observation, conducted strictly simultaneously with *XMM-Newton*, in 2013 April for cross-calibration purposes. The joint *NuSTAR* and *XMM-Newton* spectrum reveals spectral complexity, and specifically, a soft spectrum in the 2–10 keV range, hardening at the high-energy part of its bandpass. While a similar hard spectral "tail" was previously measured in the spectrum of this object by *HEAO-1* (Urry & Mushotzky 1982) as well as by *Beppo*-SAX (Giommi et al. 1998), this was done with less sensitive, non-imaging instruments; the sensitive *NuSTAR* observation allows us to reliably confirm its presence and characterize the spectrum in more detail. With relatively simple modeling of the broadband SED in the context of SSC models, we are able to draw inferences about the distribution of radiating particles over a broad range of energies.

Unless otherwise specified, we adopt the concordance cosmology, $\Omega_{\rm M} = 0.3$, $\Omega_\Lambda = 0.7$, and $H_0 = 70\,{\rm km\,s^{-1}\,Mpc^{-1}}$.

2. OBSERVATIONS AND DATA REDUCTION

Although *NuSTAR* observed PKS 2155-304 multiple times in 2013, here we report on the first observation, performed on 2013 April 23–24, or around MJD 56405. Those observations were coordinated to be strictly simultaneous with multiple X-ray instruments for the purpose of cross-calibration. The campaign, described in Madsen et al. (2016), yielded useful data from *Chandra*, *Swift*, *Suzaku*, *NuSTAR*, and *XMM-Newton*. For the purpose of the current study, we use only the *XMM-Newton* soft X-ray and the *NuSTAR* hard X-ray data, as those provided the best statistics; we also include *Swift* UVOT data to provide simultaneous optical/UV coverage towards constraining the emission models. Subsequent *NuSTAR* observations of PKS 2155-304 were conducted simultaneously with the H.E.S.S.-II Cherenkov telescope and will be reported elsewhere; for a preliminary overview, see Sanchez et al. (2015).

2.1. NuSTAR

NuSTAR, a NASA Small Explorer satellite sensitive in the hard X-ray band, features two multilayer-coated telescopes, focusing the reflected X-rays on the pixellated CdZnTe focal plane modules, FPMA and FPMB. The observatory provides a bandpass of 3–79 keV with spectral resolution of ∼1 keV. The field of view of each telescope is ∼13′, and the half-power diameter of an image of a point source is ∼1′. This allows a reliable estimate and subtraction of instrumental and cosmic backgrounds, resulting in an unprecedented sensitivity for measuring fluxes and spectra of celestial sources. For more details, see Harrison et al. (2013).

After screening for the South Atlantic Anomaly passages and Earth occultation, the 2013 April 23/24 pointing resulted in 44.9 ks of net observing time (OBSID 60002022002). The raw data products were processed with the *NuSTAR* Data Analysis Software (NuSTARDAS) package v. 1.3.1 (via the script `nupipeline`), producing calibrated and cleaned event files. Source data were extracted from a region of 45″ radius, centered on the centroid of X-ray emission, while the background was extracted from a 1.′5 radius region roughly 5′ SW of the source location. Spectra were binned in order to have at least 30 counts per rebinned channel. We considered the spectral channels corresponding nominally to the 3–60 keV energy range, where the source was robustly detected. The mean net (background-subtracted) count rates were 0.133 ± 0.002 and $0.129 \pm 0.002\,{\rm cts\,s^{-1}}$, respectively, for the modules FPMA and FPMB. The raw (not background-subtracted) counts binned on an orbital timescale are plotted in Figure 1. The source was variable from one orbit to another, although with only a modest amplitude, not exceeding 10%. We find no change in the hardness ratio of the source as a function of time, indicating that there was no significant spectral variability during the observation. Therefore, we focus here on time-averaged spectral analysis, summing the data into one deep spectral file.

2.2. XMM-Newton and Swift UVOT

XMM-Newton consists of three X-ray telescopes. Two of these focus celestial X-rays onto MOS CCD arrays, while the third uses the EPIC-pn camera. *XMM-Newton* observations of PKS 2155-304 were reduced using the *XMM-Newton* Science Analysis System (SAS) v. 14.0, with the calibration files of 2015 July 1. The reduction followed exactly the same procedures as those described in Madsen et al. (2016). The spectra were extracted from a region 20″ in radius for all three detectors, with events recorded in the inner 10″ discarded to avoid pile-up effects. The background was extracted from the

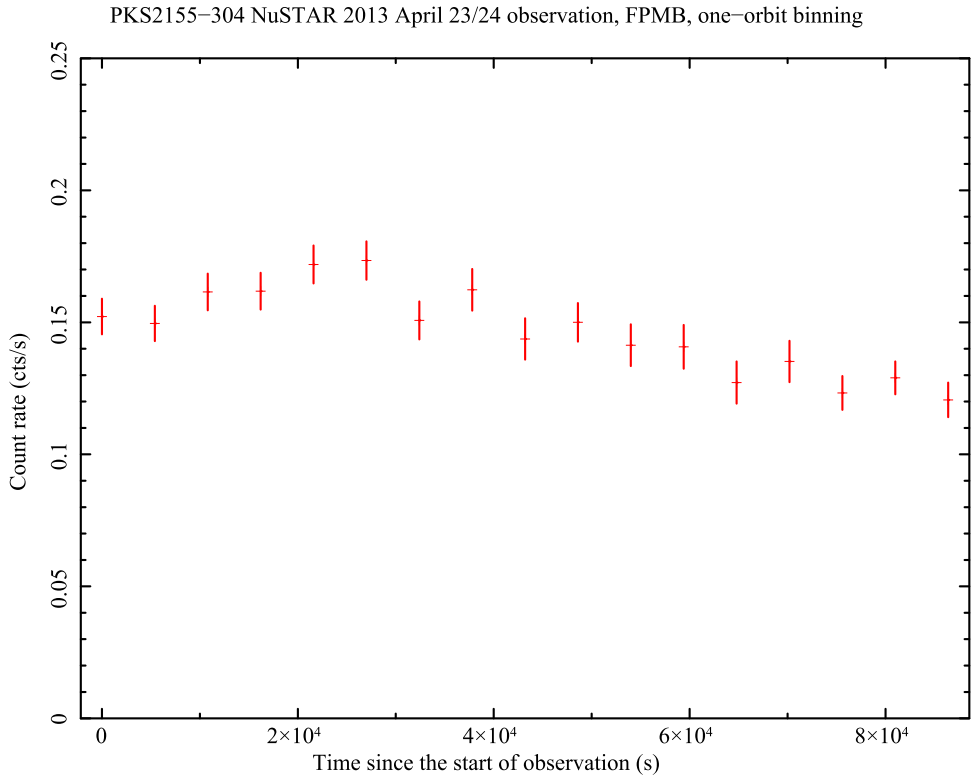

Figure 1. Light curve of PKS 2155-304, as observed by *NuSTAR* Focal Plane module "B" on 2013 April 23/24, binned on an orbital timescale.

corners of the the EPIC-pn for the `pn` data, and from the empty sky fields of the peripheral CCD for the MOS data. We considered the 0.5–10 keV energy range for spectral fitting. In this spectral range, the count rate was 2.366 ± 0.006, 2.526 ± 0.006, and 6.926 ± 0.012 counts s^{-1}, and the net exposures were 64770 s, 64770 s, and 66050 s, respectively, for the MOS1, MOS2, and `pn` cameras.

We also analyzed the *Swift* UVOT data from the pointings contemporaneous with the *NuSTAR* pointing to ensure that those are consistent with our modeling. Specifically, we measured the following de-reddened fluxes at these respective frequencies: 5.5×10^{14} Hz: $7.1 \pm 0.2 \times 10^{-11}$ erg cm^{-2} s^{-1}, 6.9×10^{14} Hz: $7.3 \pm 0.2 \times 10^{-11}$ erg cm^{-2} s^{-1}, 8.5×10^{14} Hz: $7.8 \pm 0.3 \times 10^{-11}$ erg cm^{-2} s^{-1}, 11.4×10^{14} Hz: $7.5 \pm 0.2 \times 10^{-11}$ erg cm^{-2} s^{-1}, 13.4×10^{14} Hz: $8.8 \pm 0.3 \times 10^{-11}$ erg cm^{-2} s^{-1}, and 14.5×10^{14} Hz: $8.1 \pm 0.3 \times 10^{-11}$ erg cm^{-2} s^{-1}. We include those in our modeling of the broadband spectrum in Section 4.

2.3. Fermi-LAT

The *Fermi* Large Area Telescope (*Fermi*-LAT; Atwood et al. 2009) is a pair-conversion γ-ray detector sensitive in the energy range 20 MeV to greater than 300 GeV. We analyzed the *Fermi*-LAT data with the software package `ScienceTools v10r0p5`, using the instrument response function `P8R2_SOURCE_V6` (front and back), including the Galactic diffuse emission model `gll_iem_v06`, and the isotropic background model `iso_P8R2_SOURCE_V6_v06`. Because during the *NuSTAR* observation on MJD 56405, PKS 2155-304 displayed a relatively low γ-ray state, we considered data collected over the 10 day period MJD 56400-56410, centered on the *NuSTAR* observation at MJD 56405. Gamma-ray events were selected from a region of interest within 15° of PKS 2155-304, and the background model includes all sources from the 2FGL catalog (Nolan et al. 2012) within 15° from PKS 2155-304, as well as the standard Galactic diffuse, isotropic, and residual instrumental background emission models provided by the *Fermi* Science Support Center.[23] The photon indices of all background sources were fixed.

The spectral data points were calculated by applying the unbinned maximum likelihood analysis in logarithmically spaced energy bins (with the width of the bins corresponding to the ratio of bin boundary energies of 2.512) with the photon index fixed in each bin to $\Gamma = 2$. For each bin, we set the detection criterion to require that the test statistic, or TS, $\geqslant 10$ and $N_{\rm pred} \geqslant 3$. The source was detected (TS > 10) in all energy bins in the energy range between ~250 MeV and ~15 GeV. For the bins where this criterion is not satisfied, we calculated the 95% confidence level flux upper limits (i.e., flux F such that $\log(\mathcal{L}(F)/\mathcal{L}_0) = 2$, where $\mathcal{L}_0$ is the best-fit likelihood value). (For a definition of "Test Statistics," see Mattox et al. 1996).

3. SPECTRAL FITTING

3.1. NuSTAR

The spectral fitting of all X-ray data was performed using XSPEC v12.8.2, with the standard instrumental response matrices and effective area files derived using the `ftool nuproducts`. We fitted the data for both *NuSTAR* detectors simultaneously, allowing an offset of the normalization factor for module FPMB with respect to module FPMA. Regardless of the adopted models, the normalization offset was less than

[23] http://fermi.gsfc.nasa.gov/ssc/data/access/lat/BackgroundModels.html

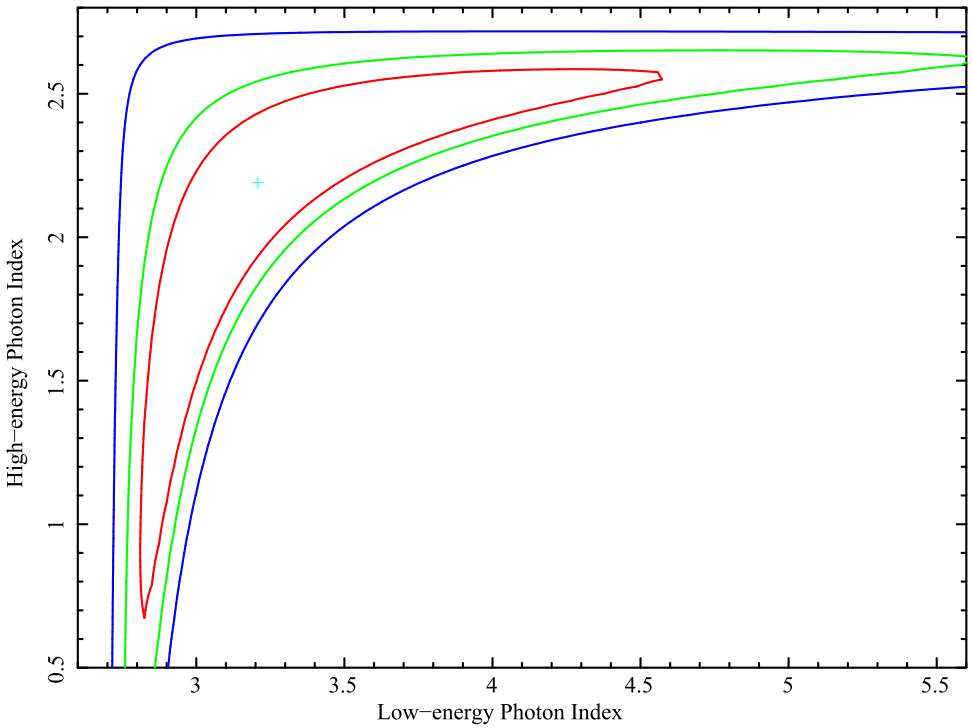

Figure 2. Confidence regions for the low- vs. high-energy power-law indices determined from the *NuSTAR* data alone. The assumed model was a superposition of two power laws. The cross corresponds to the best-fit value, while the contours from inside to outside correspond to the regions bounded by $\chi^2_{\rm min}$ + 2.7, 4.6, and 9.2.

3%. First, we adopted a simple power-law model modified by the effects of the Galactic absorption, corresponding to a column of $1.42 \times 10^{20}\,{\rm cm}^{-2}$ (Kalberla et al. 2005). While the fit is acceptable ($\chi^2 = 304$ for 295 Pulse Height Analysis, or PHA bins) and returns the power-law index of 2.73 ± 0.04, the residuals show that the *NuSTAR* spectrum is more concave (i.e., the spectrum gets flatter towards higher energies) than a simple power-law model would imply. Note that this is in contrast to previously measured spectra of two other HBL-type blazars, Mkn 421 (Baloković et al. 2016) and Mkn 501 (Furniss et al. 2015), where the $E \times F(E)$ spectra, with the *NuSTAR* data augmented by *Swift*-XRT data allowing for a broad bandpass, appear to steepen with energy.

We next attempted two more complex models (both with absorption fixed at the Galactic value as above). First, we considered a broken power law, with steeper low-energy and harder high-energy indices. The fit returned significantly improved with $\chi^2 = 297$, or $\Delta\chi^2$ of 7, for 295 PHA bins. The low- and high-energy indices are, respectively, $2.82^{+0.12}_{-0.06}$ and 2.55 ± 0.14, and the break energy is at $8.0^{+2.8}_{-2.7}$ keV. Since a broken power-law model is somewhat unphysical, we also attempted a double power-law representation of the data, also modified by Galactic absorption as above. The fit returns $\chi^2 = 292$ for 295 PHA bins with a low-energy index of $3.03^{+1.1}_{-0.25}$ and a high-energy index of 1.85 ± 0.70. Given the somewhat better value of χ^2, and since it can represent a superposition of two separate components, we express a preference for the two-power-law model. We plot the confidence regions of the low- versus high-energy indices for the two-power-law model in Figure 2. We also attempted to substitute in the place of a power law for the soft spectrum, dominating below 6 keV, a log-parabolic model where one additional parameter is added to allow for a gradual departure from a simple power law (cf. Tramacere et al. 2007). This substitution does not improve the quality of spectral fit for the *NuSTAR* data alone (but it *does* for the joint *NuSTAR* + *XMM-Newton* spectral fits; see below). Regardless of the model, the flux of the source in the 2–10 keV spectral band (chosen for easy comparison with previous observations of PKS 2155-304) is $1.1 \times 10^{-11}\,{\rm erg\,cm^{-2}\,s^{-1}}$, which is quite faint for this source, indicating that we are observing PKS 2155-304 in a very low state. For a comparison, the "low-state" of PKS 2155-304 reported by Aharonian et al. (2009) was significantly higher, ranging from ~3 to ~$9 \times 10^{-11}\,{\rm erg\,cm^{-2}\,s^{-1}}$.

In order to investigate the possibility that the apparent hardening of the spectrum of PKS 2155-304 toward higher energies is an artifact of background subtraction, the analysis was repeated with multiple background regions from various regions on the detector. Regardless of the selected region, the departure (at high energies) from the very soft, $\Gamma \sim 3$ photon index persists, and we discuss the significance in the following section.

3.2. XMM-Newton and Joint NuSTAR + XMM-Newton

We fitted all three *XMM-Newton* detectors simultaneously over the bandpass of 0.5–10 keV. These data alone can be adequately fit by a model including a simple power law + neutral absorption: the fit returned an equivalent hydrogen column of $2.6 \pm 0.2 \times 10^{20}\,{\rm cm}^{-2}$, a power-law index of 2.82 ± 0.01, and $\chi^2 = 2263$ for 2200 PHA bins. If one imposes the fixed Galactic column of $1.42 \times 10^{20}\,{\rm cm}^{-2}$, the fit is significantly worse, with $\chi^2 = 2392$ for 2200 PHA bins. This indicates that the source's soft X-ray spectrum shows significant departure from a power-law model. Motivated by previous successes in applying more complex models to describe data for HBL-type blazars such as Mkn 421 (Baloković et al. 2016) and Mkn 501 (Furniss et al. 2015),

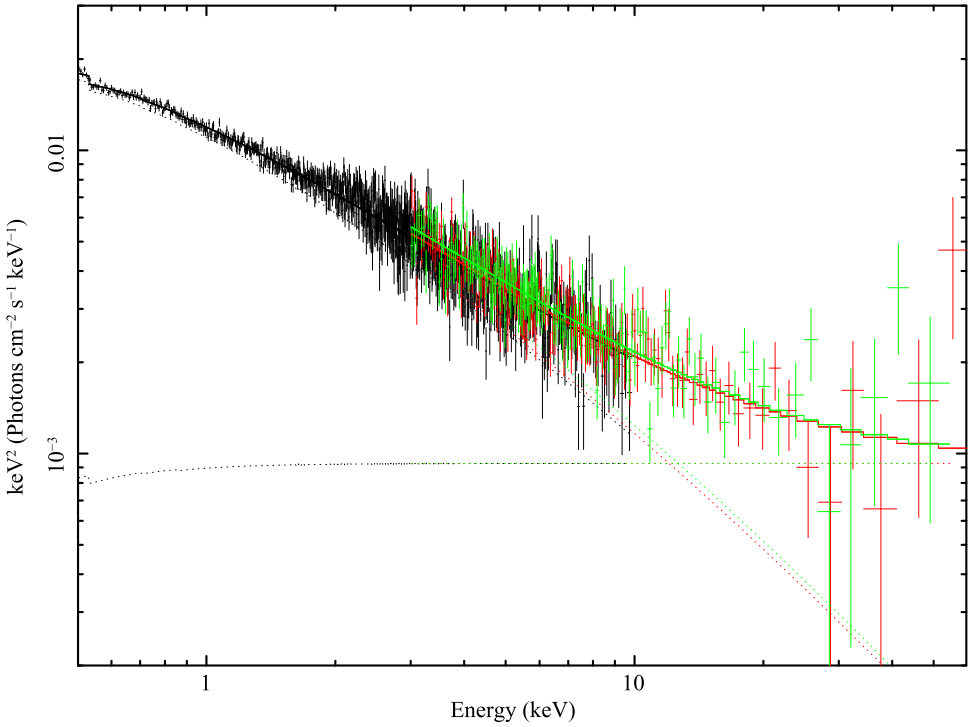

Figure 3. *XMM-Newton* pn and *NuSTAR* data for the joint observation of PKS 2155-304 on 2013 April 23–24 (the *XMM-Newton* MOS data are omitted from the plot for clarity). The solid line represents the model including the log-parabolic power-law component, plus another, hard high-energy power law; the dotted lines are the two components constituting the total model.

we next attempted a log-parabolic (logpar) model (cf. Tramacere et al. 2007). Such a model fits the data well: $\chi^2 = 2284$ for 2200 PHA bins. We chose the pivot energy E_p to be 2 keV, close to the (logarithmic) middle of the *XMM-Newton* bandpass. The fit returns the local power-law index at that energy to be 2.80 ± 0.02, with a curvature parameter β of 0.09 ± 0.02.

The strictly simultaneous observation with *XMM-Newton* and *NuSTAR* allows an unprecedented (for this source) bandpass of 0.5–60 keV, and this is the bandpass we use for subsequent fits. Motivated by the success of the logpar model above, we applied it to the joint data. We set the absorption to the Galactic value, $1.42 \times 10^{20}\,\mathrm{cm}^{-2}$, as above. With this, again setting the $E_p = 2$ keV, the best fit using all five instruments—*XMM-Newton* MOS1, MOS2, and pn as well as *NuSTAR* FPMA and FPMB—returns $\chi^2 = 2629$ for 2495 PHA bins, with the local power-law index at 2 keV of 2.78 ± 0.02, and the curvature parameter $\beta = 0.06 \pm 0.02$.

While the above fit is acceptable, motivated by evidence for the additional hard tail in the *NuSTAR* spectrum, we attempt the final model consisting of photoelectric absorption by the Galactic column and a two-component continuum modeled as logpar + hard power law. The best fit returns $\chi^2 = 2546$ for 2495 PHA bins. The local index at 2 keV is now $3.04^{+0.16}_{-0.14}$, and $\beta = 0.3^{+0.2}_{-0.1}$. For the high-energy ("hard tail") power law, the index is 2.2 ± 0.4, and its normalization (at 1 keV) is 2×10^{-3} photons $\mathrm{keV}^{-1}\,\mathrm{cm}^{-2}\,\mathrm{s}^{-1}$ (corresponding to the 20–40 keV flux of $1.4 \times 10^{-12}\,\mathrm{erg\,cm}^{-2}\,\mathrm{s}^{-1}$). Clearly, the statistical improvement to the fit is quite pronounced, mainly owing to the remarkably broad bandpass provided by the combination of *XMM-Newton* and *NuSTAR*. We present this final model in Figure 3.

To further test the significance of the hard tail, we performed a Monte Carlo simulation of the *NuSTAR* + *XMM* data, assuming just the logpar model without the power law for 1500 realizations. We found that none of the realizations were able to reproduce the feature at the observed magnitude, implying that the additional power-law component is significant at the 99.93% confidence level.

3.3. *Fermi*-LAT

During the *NuSTAR* observation on MJD 56405, PKS 2155-304 displayed a relatively low γ-ray state. As mentioned above, we considered the data collected over the 10 day period MJD 56400-56410. A binned $E > 100$ MeV γ-ray spectrum, extracted from the *Fermi*-LAT data as described above, was fitted to a simple power-law model; *Fermi*-LAT measured the photon flux above 100 MeV to be $(8 \pm 2) \times 10^{-8}\,\mathrm{ph\,s}^{-1}\,\mathrm{cm}^{-2}$ with the photon index of 1.71 ± 0.15. We plot the resulting data points as well as the fitted spectrum collected over the 10 day period in Figure 4.

4. DISCUSSION: MODELING THE BROADBAND SED AND PARTICLE CONTENT OF THE JET

In the context of the SSC models commonly invoked to explain the broadband spectra and variability of HBL-type blazars, radio-through-soft X-ray emission is commonly attributed to the synchrotron process, with X-rays being due to the most energetic electrons. The γ-ray emission is presumably produced via an inverse-Compton process; the commonly observed correlated variability in the VHE γ-ray and soft X-ray bands argues for a common energy range of the radiating particles. Most commonly invoked models to describe the broadband SEDs locate the cross-over between the

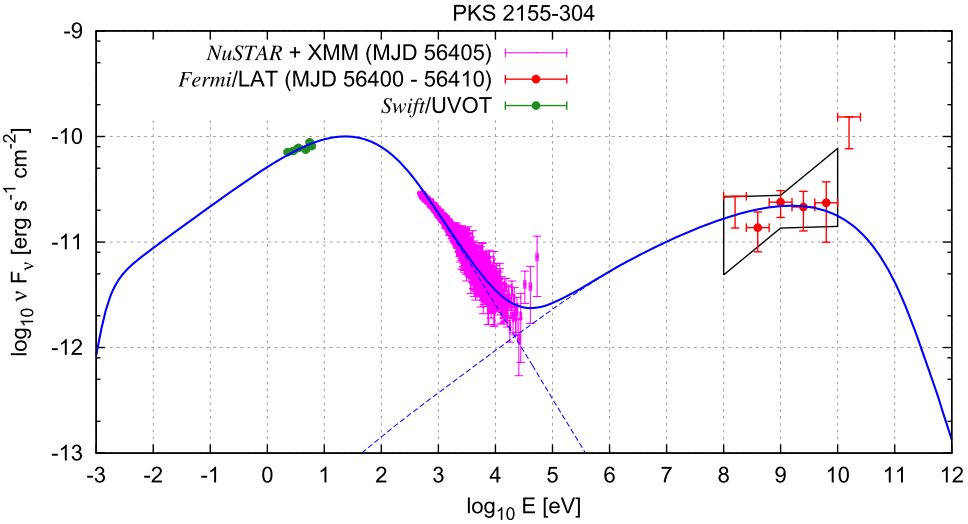

Figure 4. Spectral energy distribution of PKS 2155-304 including contemporaneous data from *Fermi*-LAT, obtained over 10 days centered on the *NuSTAR* observation (with the data points in red and a broadband spectral fit "butterfly" in black), and *NuSTAR*, *XMM-Newton* pn (magenta). Also shown is a basic SED model including synchrotron and SSC components (blue). We also plot the *Swift*-UVOT fluxes, corrected for reddening in our galaxy (green).

synchrotron and inverse-Compton peaks in the hard X-ray range, with the onset of the inverse-Compton peak manifesting itself as spectral hardening with increasing energy in the hard X-ray band. Our *NuSTAR* spectrum of PKS 2155-304 provides evidence for such spectral hardening, which we interpret as the low-energy tail of the inverse-Compton component.

We modeled the broadband SED of PKS 2155-304 using the BLAZAR code (Moderski et al. 2003). Here, the X-ray spectrum is interpreted as the high-energy end of the synchrotron component, and the γ-ray spectrum is interpreted as the inverse-Compton part of the SSC component. Our main goal is to verify a hypothesis that the spectral hardening seen in the hard X-ray band could be due to the confluence between the synchrotron and inverse-Compton components. Adopting a broken power-law distribution of injected electrons ($dN/d\gamma \propto \gamma^{-p}$ with $p = p_2$ for $\gamma_{\rm min} < \gamma < \gamma_{\rm br2}$, and $p = p_3$ for $\gamma_{\rm br2} < \gamma < \gamma_{\rm max}$), this hypothesis allows us to robustly constrain the low-energy index p_2 of the electron energy distribution, and the detailed X-ray spectrum allows us to constrain the break Lorentz factor $\gamma_{\rm br2}$ and the high-energy index p_3 of the distribution. In our basic model, we adopted the following parameters: jet Lorentz factor $\Gamma_{\rm j} = 15$, magnetic field strength $B' = 0.5$ G at a distance scale of $r = 0.065$ pc, jet half-opening angle and viewing angle $\theta_{\rm j} = \theta_{\rm obs} = 1/\Gamma_{\rm j}$, and the emitting region radius $R = 1.3 \times 10^{16}$ cm. These parameters are consistent with those inferred from previous X-ray variability studies of this source (see, e.g., Kataoka et al. 2000; Foschini et al. 2007; Katarzynski et al. 2008; Aharonian et al. 2009), but we also explored other values for $\Gamma_{\rm j}$, B', and r in order to verify that our key results do not depend on them (see below). The distribution of the Lorentz factors of the injected electrons motivated by our hypothesis is characterized by $p_2 = 2.2$, $p_3 = 3.8$, $\gamma_{\rm min} \sim 1$, $\gamma_{\rm br2} = 2.6 \times 10^4$, and $\gamma_{\rm max} \sim 10^7$. The very high value of $\gamma_{\rm max}$ is not constrained by any observational data. With this power-law index p_2, most of the electron power is contained in the lowest energy electrons, and hence the average Lorentz factor of the injected electrons is only $\langle\gamma_{\rm e}\rangle \simeq 5.6$. This model is presented in Figure 4, and it predicts the synchrotron self-absorption break at ~0.7 mm (or 1.77×10^{-3} eV).

We calculate components of the jet power required by the model as $L_q = \pi R^2 \Gamma_{\rm j}^2 u'_q c$, where u'_q is the energy density of quantity q measured in the jet comoving frame. In particular, we find the magnetic power $L_B \simeq 3.8 \times 10^{43}$ erg s^{-1}, electron power $L_{\rm e} \simeq 3.7 \times 10^{44}$ erg s^{-1}, and radiation power $L_r \simeq 1.7 \times 10^{43}$ erg s^{-1}. These values suggest that the jet composition is strongly dominated by matter with $L_{\rm e}/L_B \simeq 10$, without taking into account any protons. However, one must consider charge neutrality, so each electron must have a corresponding proton or positron. Assuming—for now—one cold proton per electron, this would predict a very high proton power of $L_{\rm p} \sim (m_{\rm p}/m_{\rm e})(L_{\rm e}/\langle\gamma_{\rm e}\rangle) \sim 1.2 \times 10^{47}$ erg s^{-1}. Providing such a large amount of kinetic power via accretion is unrealistic for an HBL-type blazar. Even if the mass of the black hole $M_{\rm BH}$ is 10^9 solar masses (not directly measured, but adopted by, e.g., Aharonian et al. 2007), and assuming high efficiency of conversion of the accretion power to jet power, in order to provide the kinetic power for the jet with an equal number of electrons and protons, the accretion rate would have to exceed the Eddington rate. Such a high accretion rate would result in an optically thick accretion disk, which in turn should reveal quasithermal components (emission lines, blue bump, and possible Compton reflection component), as commonly seen in high accretion-rate active galaxies. This is in conflict with the absence of such thermal components in HBL-type blazars (and in PKS 2155-304 in particular), which in turn suggests that HBL-type blazars accrete via inefficient, low accretion-rate, advection-dominated flows, or ADAFs (for a recent overview, see Yuan & Narayan 2014).

Alternatively, we can assume the presence of electron–positron pairs and estimate the effective numbers of leptons per proton $n_{\rm e+e-}/n_{\rm p}$. Since in any case the jet appears to be matter-dominated, we assume that the power of leptons $L_{\rm e+e-}$ originates from the dissipation of the power of protons $L_{\rm p}$, such that $L_{\rm e+e-} = \eta_{\rm diss,e} L_{\rm p}$, where $\eta_{\rm diss,e} \sim 0.1$ is the fraction of the dissipation efficiency measuring the energy fraction transferred to the leptons. Therefore, we find $n_{\rm e+e-}/n_{\rm p} \simeq (m_{\rm p}/m_{\rm e})(\eta_{\rm diss,e}/\langle\gamma_{\rm e}\rangle) \sim 33$ and $L_{\rm p} \sim 4 \times 10^{45}$ erg s^{-1}. We note that a similar constraint—but using different arguments—was obtained for the pair content in luminous blazars associated

with flat spectrum radio quasars (FSRQs) by Sikora & Madejski (2000), although their conclusions were recently somewhat weakened (Sikora et al. 2013). The problem of pair content in blazar jets was also investigated by Ghisellini (2012), and most recently, Ghisellini et al. (2014) concluded that the presence of a significant number of pairs in the powerful blazars is unlikely. In any case, FSRQ jets are unlikely to be proton-free, as jets consisting of pure pairs would overproduce the observed X-ray flux, via bulk-Compton scattering of ambient, circumnuclear photons. Since in HBL-type blazars such ambient photon fields are very weak or absent, the *minimum* proton content is basically unconstrained. We also note that, since the relative number of pairs n_{e+e-}/n_p depends only on the dissipation efficiency $\eta_{diss,e}$ and on the average electron energy $\langle\gamma_e\rangle$, our key result depends primarily on our assumptions on the energy distribution of injected pairs. Still, in order to determine the sensitivity of the resulting $\langle\gamma_e\rangle$ (which in turn determines n_{e+e-}/n_p) to our adopted Γ_j and r, we attempted two additional models. In one case, we adopted $\Gamma_j = 20$, and in another, $r = 0.13$ pc; in both cases, we kept other parameters as above, but we adjusted B' and γ_{br2} to make the model agree with the data. The resulting $\langle\gamma_e\rangle$ varied by, respectively, (roughly) -2% and $+0.5\%$ (with correspondingly small changes in n_{e+e-}/n_p), certainly not sufficient to bring this ratio close to unity. Thus, by imposing charge neutrality, a jet consisting of pure electron–proton plasma, with no positrons, is not favored.

Alternatively, we can consider a reduced number of low-energy electrons, which is basically unconstrained by the observational data. If the electrons responsible for the hard X-ray part of the SSC component ($\gamma \sim 300$) were in the fast-cooling regime, we could postulate a significantly harder low-energy power-law index $p_2 \simeq 1.2$ for the injected electron population. However, in our model the electrons are cooling efficiently only for $\gamma > 10^4$. Therefore, in order to reduce the number of low-energy electrons, it is necessary to introduce a second break in the electron injection spectrum with $p = p_1$ for $\gamma_{min} < \gamma < \gamma_{br1}$, and $p = p_2$ for $\gamma_{br1} < \gamma < \gamma_{br2}$. For example, adopting $p_1 = 1$ and $\gamma_{br1} = 100$, we have $\langle\gamma_e\rangle \simeq 84$ and $L_{e+e-} \simeq 1.5 \times 10^{44}$ erg s^{-1}, and hence $n_{e+e-}/n_p \sim 2.2$ and $L_p \sim 1.5 \times 10^{45}$ erg s^{-1}. Other possibilities, e.g., a sharp low-energy cutoff with $\gamma_{min} \sim 100$, can also be considered. In either of the above cases, assuming the presence of either electron–positron pairs or a low-energy break can bring the required jet power to reasonable values. However, without changing other parameters such as Γ_j, it is very challenging to bring the jet composition closer to equipartition, as these parameters do not affect the magnetic power L_B.

5. CONCLUSIONS

PKS 2155-304 displayed a relatively low state during the first *NuSTAR* observations of the source in 2013 April, with the measured 2–10 keV X-ray flux of only $\sim 1.1 \times 10^{-11}$ erg cm^{-2} s^{-1}, roughly three times lower than the lowest X-ray flux in 2008 August–September, reported by Aharonian et al. (2009). *NuSTAR* data reveal a steep ($\Gamma \sim 3$) spectrum below $\sim$10 keV, hardening to $\Gamma \sim 2$ above $\sim$10 keV. When fitted with strictly simultaneous *XMM-Newton* data, the soft component is best fit as a log-parabolic model, and the hard tail is even more significant. It is naturally expected that such spectral hardening as we detect in the combined *NuSTAR* and *XMM-Newton* data would be more easily detectable when the source is in a state of a relatively low soft X-ray flux. This is because the soft X-ray and VHE γ-ray variability in HBL BL Lacs is generally more rapid and has a larger amplitude than that at lower energy of the respective peaks. This is partially due to more rapid energy losses with increasing particle energy. Therefore, the chance of detecting the presumably less variable onset (low-energy end) of the inverse-Compton component is actually *greater* when the high-energy tail of the synchrotron peak is weak, and does not dilute the Compton component. Indeed, our data taken in an extremely low-flux state reveal such a component.

An application of the SSC model allows us to estimate the particle content in the jet. If we assume one proton per electron, then the total power of the jet is dominated by two orders of magnitude by particles, amounting to $L_p \sim 10^{47}$ erg s^{-1}. This would require a very large amount of power to be delivered via accretion, and would imply accretion at a highly super-Eddington rate. This, in turn, is unlikely given the absence of any quasithermal spectral components one would expect to be present in the optical/UV spectra of this source. Therefore, we consider a more plausible scenario, where the jet contains significantly more than one lepton per proton, meaning that by number, the jet is dominated by electron–positron pairs. This allows the reduction of the required jet power by two orders of magnitude, bringing it to more realistic values. The required jet power can also be reduced by introducing an additional break in the electron injection spectrum, e.g., with $\gamma_{br1} \sim 100$ and $p_1 = 1$. In either case explored here, the total power of the jet is dominated by particles rather than by magnetic fields.

In summary, while the presence of electron–positron pairs was previously postulated in relativistic jets of FSRQs (see Sikora & Madejski 2000), the new constraint from *NuSTAR* on the low-energy part of the electron distribution suggests that copious pairs may be present in jets associated with the lineless, HBL-type blazars.

The *Fermi*-LAT Collaboration acknowledges support for LAT development, operation and data analysis from NASA and DOE (United States), CEA/Irfu and IN2P3/CNRS (France), ASI and INFN (Italy), MEXT, KEK, and JAXA (Japan), and the K.A. Wallenberg Foundation, the Swedish Research Council and the National Space Board (Sweden). Science analysis support in the operations phase from INAF (Italy) and CNES (France) is also gratefully acknowledged. This work was partially supported under the NASA contract No. NNG08FD60C, and made use of observations from the *NuSTAR* mission, a project led by California Institute of Technology, managed by the Jet Propulsion Laboratory, and funded by NASA. We thank the *NuSTAR* Operations, Software, and Calibration teams for support in the execution and analysis of these observations. This research has made use of the *NuSTAR* Data Analysis Software (NuSTARDAS) jointly developed by the ASI Science Data Center (ASDC, Italy) and the California Institute of Technology (USA). K.N. was supported by NASA through Einstein Postdoctoral Fellowship grant number PF3-140130 awarded by the *Chandra* X-ray Center, and by the Polish National Science Centre grant 2015/18/E/ST9/00580. M.B. acknowledges support from NASA under the NASA Earth and Space Science Fellowship Program, grant NNX14AQ07H.

REFERENCES

Aharonian, F., Akhperjanian, A. G., Anton, G., et al. 2009, ApJL, 696, L150
Aharonian, F., Akhperjanian, A. G., Aye, K.-M., et al. 2005, A&A, 430, 865
Aharonian, F., Akhperjanian, A. G., Bazer-Bachi, A. R., et al. 2007, ApJL, 664, L71
Atwood, W. B., Abdo, A. A., Ackermann, M., et al. 2009, ApJ, 697, 1071
Baloković, M., Paneque, D., Madejski, G., et al. 2016, ApJ, 819, 156
Bhagwan, J., Gupta, A., Papadakis, I., & Wiita, P. 2014, MNRAS, 444, 3647
Brinkmann, W., Maraschi, L., Treves, A., et al. 1994, A&A, 288, 433
Chadwick, P. M., Lyons, K., McComb, T. J. L., et al. 1999, ApJ, 513, 161
Chevalier, J., Kastendieck, M. A., Rieger, F., et al. 2015, arXiv:1509.03104
Edelson, R., Griffiths, G., Markowitz, A., et al. 2001, ApJ, 554, 274
Edelson, R., Krolik, J., Madejski, G., et al. 1995, ApJ, 438, 120
Foschini, L., Ghisellini, G., Tavecchio, F., et al. 2007, ApJL, 657, L81
Furniss, A., Noda, K., Boggs, S., et al. 2015, ApJ, 812, 65
Ghisellini, G. 2012, MNRAS, 424, L26
Ghisellini, G., Celotti, A., Fossati, G., Maraschi, L., & Comastri, A. 1998, MNRAS, 301, 451
Ghisellini, G., Tavecchio, F., Maraschi, L., Celotti, A., & Sbarrato, T. 2014, Natur, 515, 376
Giommi, P., Fiore, F., Guainazzi, M., et al. 1998, A&A, 333, L5
Harrison, F. A., Craig, W. W., Christensen, F. E., et al. 2013, ApJ, 770, 103
Kalberla, P., Burton, W., Hartmann, D., et al. 2005, A&A, 440, 775
Kataoka, J., Takahashi, T., Makino, F., et al. 2000, ApJ, 528, 243
Katarzynski, K., Lenain, J.-P., Zech, A., Boisson, C., & Sol, H. 2008, MNRAS, 390, 371
Madsen, K., Beardmore, A., Forster, K., et al. 2016, ApJ, in press (arXiv:1609.09032)
Mattox, J., Bertsch, D., Chiang, J., et al. 1996, ApJ, 461, 396
Moderski, R., Sikora, M., & Błażejowski, M. 2003, A&A, 406, 855
Nolan, P., Abdo, A., Ackermann, M., et al. 2012, ApJS, 199, 31
Padovani, P., & Giommi, P. 1995, ApJ, 444, 567
Sanchez, D. A., Giebels, B., Zaborov, D., et al. 2015, arXiv:1502.02915
Schwartz, D. A., Griffiths, R., Schwarz, J., Doxsey, R., & Johnston, M. 1979, ApJL, 229, L53
Sembay, S., Warwick, R. S., Urry, C. M., et al. 1993, ApJ, 404, 112
Sikora, M., Janiak, M., Nalewajko, K., Madejski, G. M., & Moderski, R. 2013, ApJ, 779, 68
Sikora, M., & Madejski, G. 2000, ApJ, 534, 109
Tanihata, C., Urry, C. M., Takahashi, T., et al. 2001, ApJ, 563, 569
Tramacere, A., Giommi, P., Massaro, E., et al. 2007, A&A, 467, 501
Urry, C. M., & Mushotzky, R. F. 1982, ApJ, 253, 38
Urry, C. M., Treves, A., Maraschi, L., et al. 1997, ApJ, 486, 799
Yuan, F., & Narayan, R. 2014, ARA&A, 52, 529
Zhang, Y. H., Celotti, A., Treves, A., et al. 1999, ApJ, 527, 719